Applied Catalysis B: Environmental 88 (2009) 505–514

Contents lists available at ScienceDirect

Applied Catalysis B: Environmental

journal homepage: www.elsevier.com/locate/apcatb

Tailoring and structure of PtRu nanoparticles supported on functionalized carbon for DMFC applications: New evidence of the hydrous ruthenium oxide phase

J.L. Gómez de la Fuente [a], M.V. Martínez-Huerta [a,*], S. Rojas [a], P. Hernández-Fernández [b], P. Terreros [a], J.L.G. Fierro [a], M.A. Peña [a]

[a] Instituto de Catálisis y Petroleoquímica (CSIC), C/Marie Curie 2, E-28049 Madrid, Spain
[b] Dpto. Química Física Aplicada, Universidad Autónoma de Madrid, Campus UAM, E-28049 Madrid, Spain

ARTICLE INFO

Article history:
Received 29 July 2008
Received in revised form 14 October 2008
Accepted 18 October 2008
Available online 6 November 2008

Keywords:
Electrocatalyst
Methanol
PtRu
Functionalized support
$RuO_2{\cdot}xH_2O$
Hydrous ruthenium oxide
Fuel cell

ABSTRACT

The influence of the structure and morphology of PtRu nanoparticles supported on functionalized carbon black has been investigated for CO and methanol electrooxidation in a half-cell and in a DMFC single cell. Carbon black was treated with HNO_3 to obtain an oxidized surface (Vulcan-N), and PtRu nanoparticles supported on Vulcan-N were prepared via impregnation, Bönnemann's method and the sulfito-complex route. Temperature programmed reduction (TPR) measurements evidence the presence of $RuO_2{\cdot}xH_2O$ phase in the catalyst obtained by the sulfito-complex route. This phase was stabilized by metal–support interaction, whereas alloy characteristics were estimated for PtRu catalyst obtained by impregnation and Bönnemann's method. The nature of the precursor–support interaction, induced by the nature of the functional groups on the carbon surface, affects the structure of the electrocatalyst and subsequent behavior in electroactivity. When synthesized through Bönnemann's method, the surface oxygen-containing groups of the support seem to be unable to stabilize the anhydrous precursors of platinum and ruthenium, yielding crystalline RuO_2. Methanol electrooxidation performance was clearly different in the three catalysts, whereas only a few negligible differences were observed in CO oxidation. The superior performance in DMFC of the catalysts obtained by the sulfito-complex route accounts for both the presence of $RuO_2{\cdot}xH_2O$ species and the functionalization of carbon black.

1. Introduction

Fuel cells are an emerging technology that can meet the demand for energy in today's society. Direct methanol fuel cells (DMFC) have emerged as very promising devices for providing energy with high efficiency because of convenient fuel feeding and easy operation at low temperature [1–3]. However, the success of fuel cell technology depends largely on the electrocatalyst. With regard to DMFC anode catalysts, carbon-supported PtRu catalysts are commonly employed for the electrooxidation of methanol; however, two major challenges for commercial applications still remain: cost reduction and catalytic performance (including activity, consistency and durability) [4,5]. Research into resolving these drawbacks is focused on increasing the electroactive surface area and accessibility to active sites. The design of advanced electrocatalysts relies mainly on the "bifunctional approach" [6], in which the role of Ru promoter is to dissociate water creating oxygenated species, which in the presence of Pt oxidize CO to CO_2. The role of electronic factors should not be underestimated either.

Over the past 10 years, numerous approaches have been adopted in order to understand the nature of these bimetallic catalysts, including different catalyst preparation methods and carbon supporting strategies. The preparation of carbon-supported PtRu catalysts is usually based on supporting metal precursors on carbon followed by their transformation into metal particles. Impregnation [7–12] and colloidal methods [13,14] are among the most important synthetic routes used. Either method comprises a chemical step to forming nanoparticles, and a depositing step for dispersing them onto the carbon particles. Carbon black is often employed as support for noble metals in the electrodes of solid polymer fuel cells. Designing an appropriate catalyst implies an optimal selection of both the support and the synthesis method of the active component.

The oxidation state of the Ru component is still a topic of discussion. While some authors refer to the active ruthenium compound mainly as metallic Ru^0 in a bimetallic alloy [15–17], early research revealed that hydrous ruthenium oxide as a part of bimetallic PtRu electrodes is the most active catalyst for methanol

* Corresponding author. Tel.: +34 915 854 778; fax: +34 915 854 760.
E-mail address: mmartinez@icp.csic.es (M.V. Martínez-Huerta).

0926-3373/$ – see front matter © 2008 Elsevier B.V. All rights reserved.
doi:10.1016/j.apcatb.2008.10.016

oxidation [9,18–22]. According to this latter point, Rolison and coworkers [18,19] emphasized the importance of hydrous ruthenium oxides because the $RuO_2{\cdot}xH_2O$ speciation of Ru in nanoscale PtRu blacks records both high electron and high proton conductivity, which results in a much more active catalyst for methanol oxidation. Recently, Cao et al. [21] reported that a new nanocomposite $Pt/RuO_2{\cdot}xH_2O$ supported on carbon nanotubes presented higher activity in methanol electrooxidation as compared to that of PtRu commercial catalysts. The superior performance was attributed to the presence of $RuO_2{\cdot}xH_2O$ species. However, direct evidence of the catalytic function of hydrous oxides is scarce.

It is well known that the presence of oxygen surface groups influences the surface behavior of carbons to a great extent [23–25]. Our team have studied the effect of the oxygenated surface groups of carbon support on the electrochemical properties of PtRu catalysts [10,26]. We have revealed how the treatment of carbon with oxidizing reagents improves the activity of the electrocatalyst in methanol electrooxidation. However, the reason for the enhanced performance has not been fully determined.

The purpose of the present work is to obtain a deeper insight into the nature of carbon-supported PtRu electrocatalysts for methanol electrooxidation. Accordingly, a comparative study of PtRu/C catalysts of different genesis was carried out, using carbon black functionalized with HNO_3 as support. Since tailoring the appropriate catalyst for methanol electrooxidation implies an optimal selection of the synthesis method of the active components, an impregnation method [10] and two different colloidal procedures – the sulfito-complex route [13] and Bönnemann's method [14] – were used for the study. Special emphasis was placed on metal–support interaction determined by the nature of functional groups at the carbon surface and on determining the nature of Ru phases, as these factors strongly affect subsequent catalyst behavior. Electrocatalysts were extensively characterized using different physicochemical and electrochemical techniques. Additionally, this work illustrates how temperature programmed reduction (TPR) analyses facilitate a good understanding of the nature of Pt and Ru nanoparticles, as regards the performance of the electrocatalysts in a practical DMFC.

2. Experimental

2.1. Catalyst preparation

A commercial carbon black Vulcan XC 72R was used as support, and it was functionalized with HNO_3 to obtain an oxidized surface, as previously described [10]. This sample was called Vulcan-N, while non-treated carbon was referred to as simply Vulcan. Different electrocatalysts with 20 wt% PtRu (1:1) supported on carbon have been prepared by impregnation and two different colloidal methods.

(a) *Impregnation method* [10]: The Vulcan-N was impregnated with an aqueous solution of H_2PtCl_6 (120 mM) and $RuCl_3$ (40 mM) precursors at 85 °C, mixed with half its volume of isopropanol. The mixture was reduced with an excess of formaldehyde, filtered, washed with hot water and dried overnight at 110 °C. The electrocatalyst obtained was called IPR20-N (PtRu/Vulcan-N).

(b) *Bönnemann's method*: This synthesis method is based on the colloidal procedure described by Bönnemann et al. [14] and was performed with the rigorous exclusion of air and moisture under nitrogen using standard vacuum-line and Schlenk techniques. First of all, the reducing agent $NOct_4[BEt_3H]$ was prepared from $NOct_4Br$ and $K[BEt_3H]$ in THF. A solution of $NOct_4[BEt_3H]$ in THF (0.16 M) was then added to a vigorously stirred suspension of $PtCl_2$ (1 mM) and $RuCl_3$ (1 mM) in THF at 40 °C. The resulting suspension was stirred for 16 h. Acetone was added to remove the excess reducing agent. The colloidal suspension was added dropwise over a suspension of Vulcan-N in THF under vigorous stirring. After 12 h, absolute ethanol was added. Subsequently, the solid was filtered and washed with ethanol to remove organic sub-products. Finally, the electrocatalyst was dried overnight in air at 110 °C. The obtained sample was called BPR20-N (PtRu/Vulcan-N).

(c) *Sulfito-complex route*: This synthesis is based on the procedure described by Watanabe et al. [13]. Basically, a solution of H_2PtCl_6 (50 mM) in water was reduced by adding a solution of $Na_2S_2O_5$ (284 mM) in water to obtain a colorless solution, which was then oxidized with H_2O_2 (30%, v/v). During the addition, the pH was adjusted to close to 5 by adding Na_2CO_3. A solution of $RuCl_3$ (110 mM) in water was added dropwise under continuous stirring. Carbon black supports (Vulcan or Vulcan-N) were added to the solution under constant stirring, and hydrogen gas was then bubbled through the mixture for 1 h. It was then allowed to settle, filtered and washed with hot water. The solids thus obtained were dried in air at 110 °C for 17 h. The electrocatalysts were called CPR20 (PtRu/Vulcan) and CPR20-N (PtRu/Vulcan-N).

A reference sample of $RuO_2{\cdot}xH_2O$ was prepared by precipitation from an aqueous solution of $RuCl_3$ with aqueous NaOH at pH 10 and 65 °C [27]. Another reference sample of RuO_2 was prepared from Ru/Vulcan catalyst (obtained by the impregnation method (a)), and then calcined in an air flow at 800 °C.

2.2. Physicochemical characterization

Thermogravimetric analysis (TGA) under controlled atmosphere was carried out on a Mettler Toledo TGA/SDTA851e, using 200 $cm^3\,min^{-1}$ of N_2 as carrier gas, 20 $cm^3\,min^{-1}$ of oxygen as reactive gas, and a heating rate of 10 °C min^{-1}. Total-reflection X-ray fluorescence (TXRF) was performed on a Seifert EXTRA-II spectrometer equipped with two X-ray fine focus lines, Mo and W anodes, and a Si(Li) detector with an active area of 80 mm^2 and a resolution of 157 eV at 5.9 keV (Mn Kα). The Pt/Ru atomic ratio was determined by using Pt$L\alpha$ and Ru$L\alpha$ emission lines in the XRF spectra after proper calibration with standard samples.

Textural properties have been evaluated by N_2 adsorption–desorption isotherms of the samples, recorded at −196 °C with a Micromeritics ASAP 2000 apparatus. Samples were previously degassed at 150 °C for 24 h. Specific areas were calculated by applying the BET method within the $0.05 < P/P_0 < 0.30$ relative pressure range.

Metal phases have been determined by using X-ray diffraction (XRD) measurements. X-ray diffraction powder patterns were obtained on a Seifert 3000P X-ray diffractometer, using a Cu Kα-source. The powder diffractograms of the samples were recorded from 15° to 95° with a scanning rate of 0.04° s^{-1}.

Particle size and morphology as well as PtRu dispersion of the samples were evaluated from the transmission electron microscopy (TEM) images obtained in a Jeol 2000FX microscope operating with an accelerating voltage of 200 kV. Typically, 10 mg of the sample were dispersed in acetone in an ultrasonic bath for 15 min. The sample was then placed on a Cu carbon grid where the liquid phase was then evaporated.

Photoelectron spectra (XPS) were obtained with a VG Escalab 200R spectrometer equipped with a hemispherical electron analyzer (pass energy of 20 eV) and an Mg Kα ($h\nu$ = 1253.6 eV, 1 eV = 1.6302×10^{-19} J) X-ray source, powered at 120 W. The

binding energies were calibrated relative to the C 1s peak from carbon contamination of the samples at 284.6 eV. High-resolution spectra envelopes were obtained by curve-fitting synthetic peak components using *XPSpeak 4.1* software.

FTIR Spectra were recorded in the 4000–400 cm^{-1} region with a Nicolet 5ZDX spectrometer using KBr pellets, with 512 scans recorded at a resolution of 4 cm^{-1}.

Temperature programmed reduction (TPR) analyses were recorded on a Micromeritics TPR/TPD 2900 apparatus with a thermal conductivity detector (TCD). Typically, 30 mg of the sample with a granular size between 590 and 425 μm were mounted on a quartz tubular U-shaped reactor and warmed from r.t. to 500 °C at 10° min^{-1} under 50 mL min^{-1} of 10% H_2/Ar flow. Previously, the samples were dried under 50 mL min^{-1} He at 110 °C for 1 h.

2.3. Electrochemical characterization in half-cell

The electrochemical measurements were carried out in a standard three-electrode electrochemical cell at room temperature. The electronic equipment consisted of a Radiometer Analytical Model PGZ 301 potentiostat. A glassy carbon electrode (0.071 cm^2) was used as working electrode, being prepared according to a modified method developed by Schmidt et al. [28]. Typically, 3.5 mg of the electrocatalyst were dispersed in Mili-Q water (1 mL) and Nafion (30 μL) in an ultrasonic bath for 45 min. Aliquots of 5 μL of the ink were deposited onto the electrode and dried over an Ar flow for 30 min. All the potentials were referenced to the normal hydrogen electrode (NHE) and measured versus an Hg/Hg_2SO_4 electrode. A Pt wire was used as the counter electrode. The electrolyte was purged with purified argon prior to each experiment. In order to clean and activate the electrode surface, cyclic voltammetry (CV) in 0.5 M H_2SO_4 was performed. The samples were cycled at 20 mV s^{-1} between 0 and 0.8 V (20 cycles), and a further cycle at 25 mV s^{-1} between 0 and 1.15 V was recorded. Adsorbed CO (CO_{ad}) was measured by CO stripping voltammetry in 0.5 M $HClO_4$ solution. Gaseous CO was fed into the cell for 12 min while maintaining a constant voltage of 0.02 V. After CO removal (Ar purge for 30 min), the working electrode was subjected to a cyclic voltammetry step at a 10 mV s^{-1} scan rate, and 3 consecutive cycles were recorded. The amount of adsorbed CO was evaluated by integration of the CO stripping peak, corrected for the electric double-layer capacitance. The surface area was estimated assuming a monolayer of linearly adsorbed CO and the charge necessary for its oxidation as 420 μC cm^{-2}. The electrocatalytic activity of catalysts for methanol oxidation was studied in 0.5 M H_2SO_4 + 2 M CH_3OH by cyclic voltammetry at 20 mV s^{-1} between 0 and 0.8 V.

2.4. DMFC testing

The electrochemical activity of the PtRu/C samples as anode catalysts in DMFC was evaluated. Pt/C (Johnson Matthey, 40 wt% Pt) was used as the cathode electrode. The platinum loading was 2 mg cm^{-2} for the anode and 3 mg cm^{-2} for the cathode. A commercial Nafion 117 membrane (Dupont) was treated to clean and protonate its surface. The catalyst layer was sprayed onto the membrane by means of an ink. The ink generally consisted of isopropanol (Merck), Mili-Q water, Nafion solution (5 wt% Aldrich) and catalyst powders. Once the ink had been sprayed onto the electrolyte (three-layered structure), the MEA was obtained by hot pressing a Teflon treated carbon cloth (Electrochem. Inc.), used as gas diffusion layer, onto both sides of the anode–membrane–cathode assembly at 123 °C and residual press for 3 min [29].

The DMFC was assembled by mounting the MEA into a single cell with an active cross-sectional area of 5 cm^2 (Electrochem. Inc.). The single cell was initially activated at open circuit maintaining the following operating conditions for 30 min: anode fuel, H_2; flow rate, 100 mL min^{-1}; oxygen flow rate, 100 mL min^{-1}; oxygen and hydrogen pressure, 3 bar; oxygen and hydrogen humidity, saturated at 60 °C; cell temperature, 45 °C [30]. After the activation process, the DMFC was tested by feeding methanol 2 M at a flow rate of 3 mL min^{-1} using a high-pressure pump (Gilson 307). The methanol solution was heated at 80 °C. The oxygen was fed into the cathode inlet at a flow rate of 200 mL min^{-1} and a pressure of 3 bar. Polarization curves were recorded at 90 °C by fixing the load current, which was controlled by an electric load system (Electrochem. Inc. ECL150). All single cell tests were conducted three times to ensure the repeatability of the measurement.

3. Results and discussion

3.1. Characterization of carbon support

The treatment of the support Vulcan XC 72R with HNO_3 (Vulcan-N) generates an intense surface oxidation observed by TPD experiments described previously [10]. BET areas of the carbon samples are listed in Table 1. Although the specific surface area values decrease with nitric acidic treatment, no other differences in textural properties evaluated by N_2 adsorption–desorption isotherms were found. It has been reported that the treatment of carbons with HNO_3 does not affect their physical morphology but alters their surface chemical properties, and that HNO_3 treatment is the most effective acid reagent for creating acidic carbon groups [31].

FTIR is a very useful and direct technique for studying the nature of oxygen surface groups. An inspection of the FTIR spectra of supports, Fig. 1, shows that the treatment of Vulcan with HNO_3

Table 1
Physicochemical parameters of the electrocatalysts based on analysis of TXRF, TGA, BET, XRD and TEM.

Sample	Pt:Ru[a]	PtRu, wt%[b]	BET (m^2 g^{-1})	Particle size (TEM)
Vulcan XC 72R			203	
Vulcan-N			159	
IPR20-N	1:0.8	21	158	3.7
BPR20-N	1:0.8	18	82	2.3
CPR20-N	1:1	21	155	2.2

[a] Atomic ratio from TXRF.
[b] From TGA and TXRF.

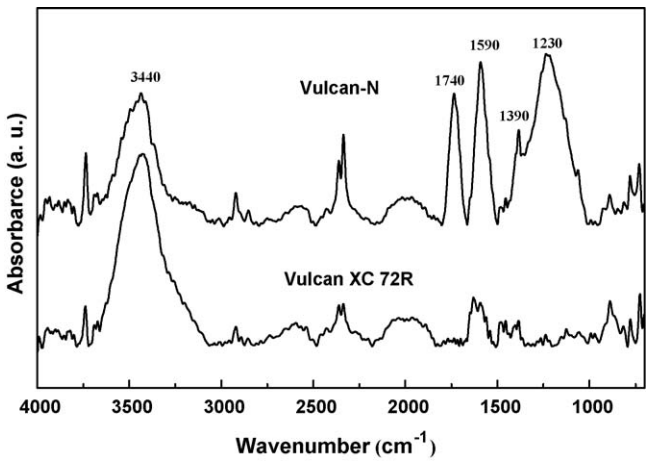

Fig. 1. FTIR spectra of Vulcan XC 72R and Vulcan-N.

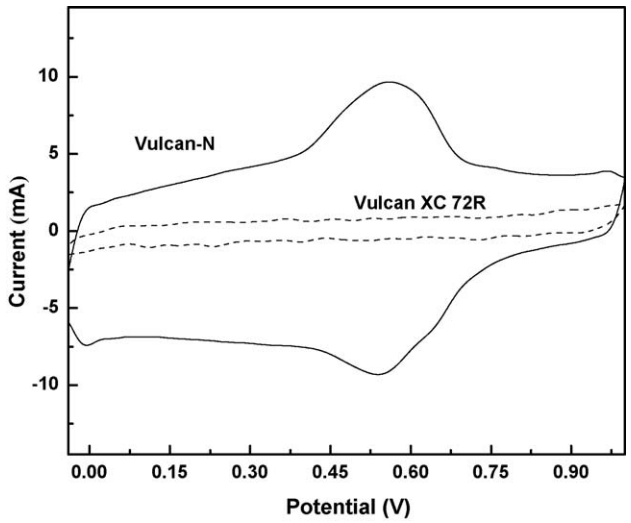

Fig. 2. Cyclic voltammetry of supports in 0.5 M H_2SO_4 at 25 °C, $v = 0.02\,V\,s^{-1}$.

generates four bands of interest: (i) ~1740 cm^{-1}, associated with C=O stretching in lactones and carboxylic groups; (ii) ~1590 cm^{-1}, associated with aromatic stretching mode, quinonic structures and carboxylate groups; (iii) ~1390 cm^{-1}, associated with –O–H bending vibrations in phenolic and carboxylic OH; and (iv) a broad band centered around ~1230 cm^{-1} associated with C–O stretching vibrations, and which could indicate the existence of aromatic ethers, such as lactonic structures, phenols and carboxylic groups [32,33].

In order to characterize the electroactive surface oxides, the cyclic voltammetry of the supports was recorded (Fig. 2). The cyclic voltammetry of Vulcan-N shows evidence of surface oxidation due the presence of one anodic peak current at −0.55 V. This peak is assigned to the hydroquinone–quinone redox couple (HQ/Q) [34].

3.2. Characterization of electrocatalysts

The physicochemical parameters of the electrocatalysts based on the analysis of TXRF, TGA, BET, XRD and TEM are shown in Table 1. The atomic ratio Pt:Ru (from TXRF) is approximately 1:1 in all catalysts. PtRu wt% values are determined from atomic ratio PtRu and TGA based on the methodology described elsewhere [10].

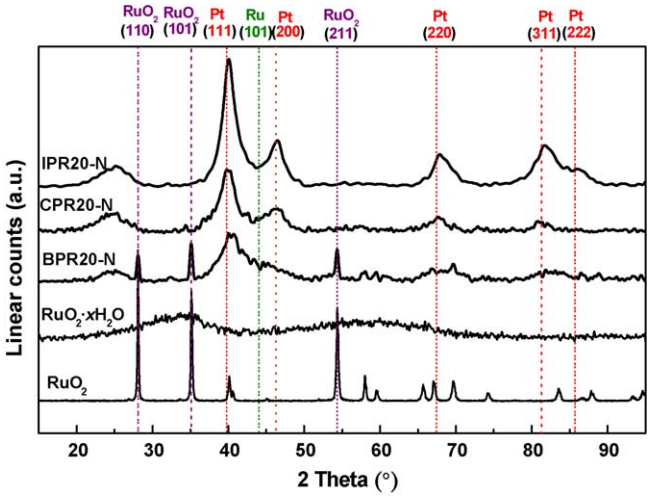

Fig. 3. X-ray diffractograms of catalysts, $RuO_2{\cdot}xH_2O$ and RuO_2.

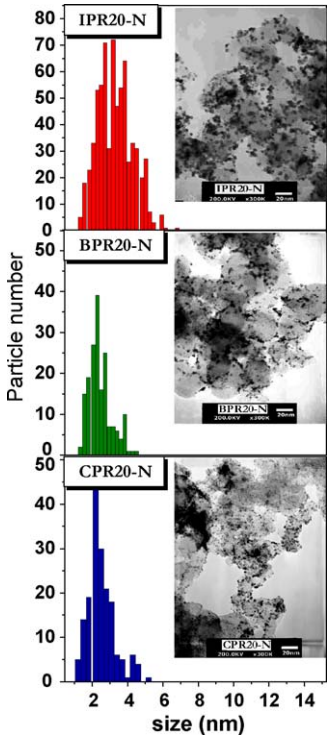

Fig. 4. TEM images and the corresponding histograms for electrocatalysts (magnification 300k×).

BET specific area is similar in all catalysts, except in BPR20-N, which decreases sharply.

X-ray diffractograms of catalysts are shown in Fig. 3. The diffraction patterns of $RuO_2{\cdot}xH_2O$ and RuO_2 are also included in Fig. 3 for comparison. All catalyst patterns display diffraction lines of Pt fcc (JPCDS 04802) and the characteristic diffraction pattern of graphitic carbon (24.9°, 43.3° and 79.6°). The diffractograms of the electrocatalyst prepared by Bönnemann's method and by the impregnation method show a slight shift to higher 2θ values with respect to the same reflections of the Pt fcc structure. This shift in the Pt peak position could be attributed to a higher degree of alloying between Pt and Ru in IPR20-N and BPR20-N catalysts [16]. Additionally, BPR20-N catalyst shows XRD peaks ascribed to the (1 1 0), (1 0 1) and (2 1 1) planes of the tetragonal RuO_2 structure (JPCDS 73-1469). The intensity of the diffraction lines of Pt fcc of CPR20-N and BPR20-N catalysts decreased due to the low crystallinity of the nanoparticles of Pt. Moreover, no peaks were observed for the hexagonal close-packed (hpc) Ru phase or $RuO_2{\cdot}xH_2O$.

Fig. 4 shows transmission electron microscopy images and the corresponding histograms. The particle size distribution of the samples prepared by colloidal routes is narrower than that observed for the catalysts prepared by impregnation. CPR20-N and BPR20-N catalysts present average particle sizes of 2.2 nm, while for IPR20-N it is 3.7 nm (Table 1). This is consistent with the literature, where colloidal methods allow for the synthesis of PtRu catalyst with higher specific surface area resulting in the easy control of particle size and distribution [4]. In general, there is a homogeneous distribution of particles, although regions displaying a certain agglomeration of PtRu nanoparticles are also observed. These observations are in line with previous studies on functionalized carbon as support [10,26].

Photoelectron spectroscopy (XPS) was used to define the oxidation states of the metal nanoparticles in the electrocatalysts (Table 2). The Pt4f signal (Fig. 5) could be resolved into three

Table 2
Binding energies (eV) of core levels and Pt/Ru atomic ratio of electrocatalysts.

Catalyst	Pt species	BE of Pt4f$_{7/2}$ (eV)	Ru species	BE of Ru3p (eV)	Atomic ratio Pt/Ru
IPR20-N	Pt^0	71.6 (47)	Ru^0	461.4 (6)	1.0
	Pt^{2+}	72.8 (44)	Ru^{4+}	463.2 (74)	
	Pt^{4+}	74.7 (9)	Ru^{4+}(hydrated)	466.4 (20)	
BPR20-N	Pt^0	71.6 (42)		461.2 (8)	2.0
	Pt^{2+}	72.9 (41)	Ru^{4+}	463.4 (76)	
	Pt^{4+}	74.8 (17)	Ru^{4+}(hydrated)	466.9 (16)	
CPR20-N	Pt^0	71.9 (18)			0.8
	Pt^{2+}	73.1 (43)	Ru^{4+}	463.6 (70)	
	Pt^{4+}	74.7 (38)	Ru^{4+}(hydrated)	466.5 (30)	

doublets in all electrocatalysts. The Pt 4f$_{7/2}$ component at 71.6–71.9 eV is attributed to metallic Pt. The Pt^0 peak is the most intense component in IPR20-N and BPR20-N (ca. 45%), and the least intense component in CPR20-N (18%). The Pt 4f$_{7/2}$ component of the second doublet observed at 72.8–73.1 eV can be assigned to Pt(2+) in PtO and $Pt(OH)_2$-like species [35]. A similar contribution was observed in all samples (~40%). An additional Pt peak at BE ca. 74.7 eV corresponding to a higher oxidation state Pt(4+) is also observed. In CPR20-N, these species are particularly intense, and their relative abundance accounts for 38% of total Pt loading. In the case of ruthenium, the Ru3p signal was deconvoluted into three distinguishable doublets of different intensity in IPR20-N and BPR20-N, and two doublets in CPR20-N (Fig. 6). The peak at BE 461.2–461.4 eV in IPR20-N and BPR20-N was attributed to Ru^0 [35], while the two peaks at higher BE in all catalysts were assigned to anhydrous RuO_2 (463.2–463.6 eV), and hydrous amorphous $RuO_2{\cdot}xH_2O$ (466.4–466.9 eV) [36]. The presence of the RuO_3 phase was excluded in favor of the hydrous amorphous $RuO_2{\cdot}xH_2O$, since the former is thermodynamically unstable under the reaction conditions employed here [19]. It is noteworthy that the contribution of hydrous amorphous $RuO_2{\cdot}xH_2O$ is higher in CPR20-N than in IPR20-N and BPR20-N. Surface traces of sulfur in CPR20-N were observed. S 2p signal displays two components, a small one at 164.0 eV assigned to $-\mathbf{S}^*SO_3^-$ from $Na_2S_2O_5$, and a more intense peak at 168.4 eV ($-S\mathbf{S}^*O_3^-$ from $Na_2S_2O_5$, or $\mathbf{S}O_3H^-$ from $HNaSO_3$) [37]. The surface Pt/Ru ratio, determined by XPS, is 0.8 for CPR20-N, but increases to 1.2 in IPR20-N and 2.1 in BPR20-N. Accordingly, a higher surface enrichment of Ru takes place in a catalyst obtained by the sulfito-complex route.

FTIR spectra of the catalysts and Vulcan-N are shown in Fig. 7. The spectra of IPRN-20 and CPR20-N display the most significant differences with respect to Vulcan-N. There is a sharp decrease in the intensity of bands at 1000–1400 cm^{-1} and ~1740 cm^{-1} associated with the existence of lactones, phenols, aromatic ethers and carboxylic groups [32,33]. Furthermore, CPR20-N has two additional bands at 1187 and 1110 cm^{-1} associated with S=O and R–O–SO^{3-}, respectively, due to the presence of $Na_2S_2O_5$. The differences between the FTIR spectra of CPR20-N and IPR20-N with respect to Vulcan-N support could reflect a certain degree of interaction between metal and the oxygen-containing surface groups of the support. The ability of such groups to stabilize metal nanoparticles on a carbon surface is a topic of much debate. FTIR spectra results are in line with this hypothesis, although the nature

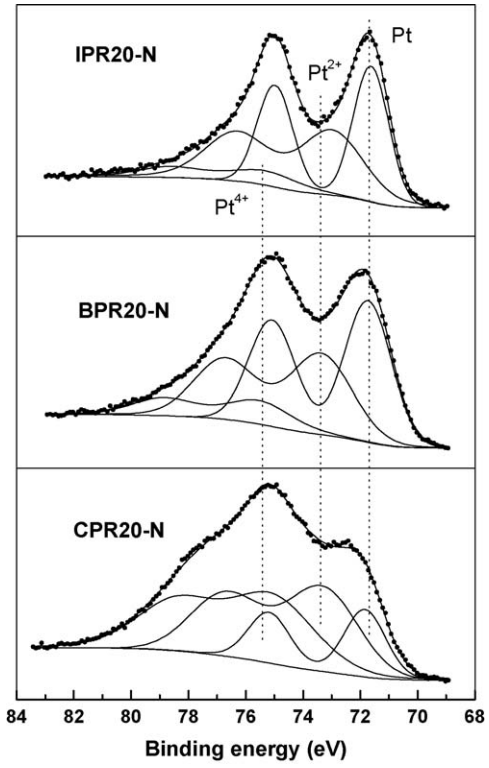

Fig. 5. XPS Pt4f core-level of the electrocatalysts.

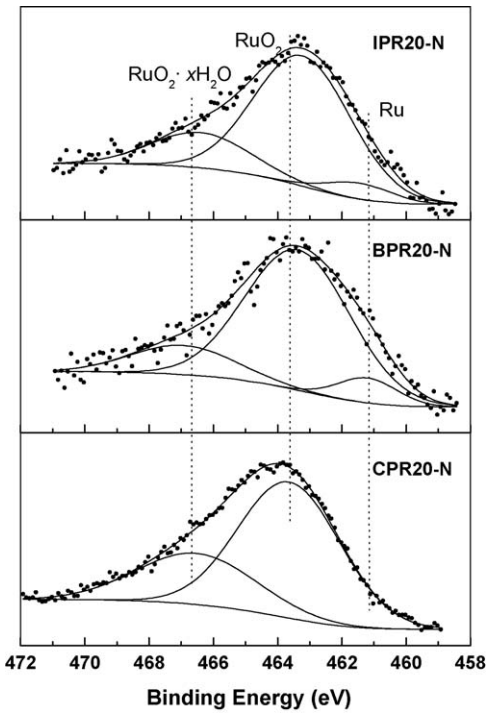

Fig. 6. XPS Ru3p core-level of the electrocatalysts.

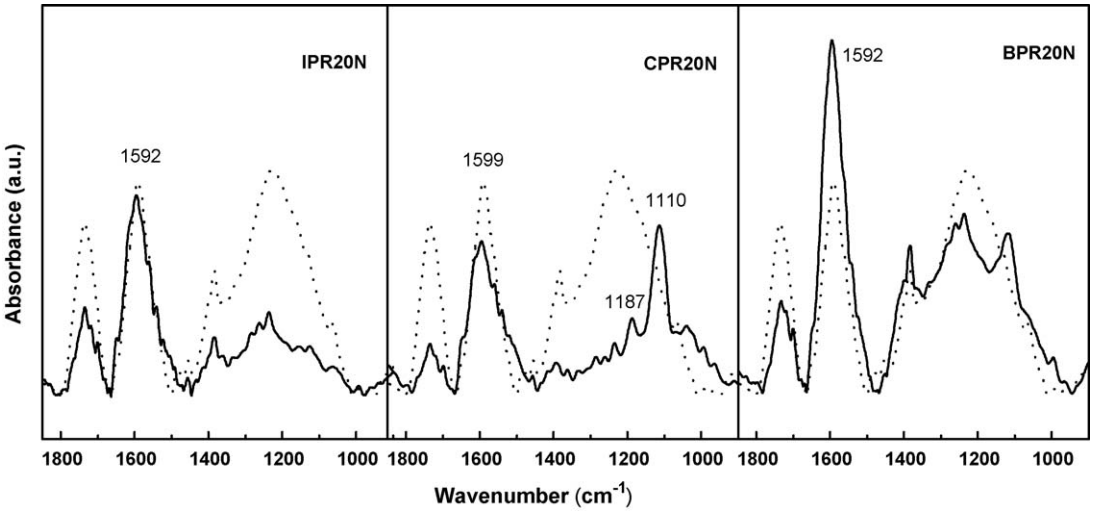

Fig. 7. FTIR spectra of support Vulcan-N (dash) and electrocatalysts (solid).

of this metal–support interaction cannot be clarified. Impregnation and sulfito-complex methods employ aqueous solutions of the same metal precursors (H_2PtCl_6 and $RuCl_3$). However, $PtCl_2$ and $RuCl_3$ in anhydrous conditions and non-polar solvents are employed in Bönnemann's method. These differences affect metal precursor distribution throughout the carbon support, where the solvent–carbon interaction may play an important role. It seems that the functionalized support is unable to stabilize the anhydrous precursors of platinum and ruthenium in a catalyst obtained by Bönnemann's method.

The composition of PtRu nanocrystallites has been explored by using the temperature programmed reduction (TPR) technique. The TPR technique may be a surface-sensitive detector for probing the surface composition of bimetallic particles deposited on PtRu/C catalysts [8,38]. Metal oxides are reduced by flowing hydrogen according to the following reaction pathway

$$MO_x + xH_2 \rightarrow xH_2O + M$$

The TPR profiles of electrocatalysts supported on Vulcan-N, reference Ru samples, and reference catalyst CPR20 (supported on untreated Vulcan XC 72R) are shown in Fig. 8. All samples were heat-treated under air at 110 °C for ca. 17 h. Prior to the TPR analysis, samples were dried under He at 110 °C for 1 h. As depicted in Fig. 8, the TPR profile is characteristic of each catalyst. Vulcan-N support shows no hydrogen consumption features. Furthermore, no hydrogen consumption peaks are observed on the catalyst prepared by the impregnation method (IPR20-N). Recent TPR studies of PtRu nanoalloys dispersed on active carbon revealed that the temperature required for the reduction varies with their surface composition [8]. A Pt-rich surface has a reduction temperature ~ −3 °C. A Ru-rich surface displays a higher reduction temperature (~47 °C). Since the equipment used for this work does not allow for analysis below 25 °C, the presence of a Pt-rich surface of PtRu nanoalloys cannot be ruled out. Fig. 8B depicts the TPR profiles of BPR20-N and RuO_2. BPR20-N has two reduction peaks at 157 °C and 267 °C, whereas RuO_2 records a single hydrogen consumption peak at 169 °C. The peak at 267 °C was assigned to the presence of remaining platinum precursor [39]. The reduction peak at 157 °C can be assigned to the reduction of RuO_2. The presence of RuO_2 is further confirmed by means of XRD, as described above. The shifting of the reduction temperature from 157 °C in BPR20-N to 169 °C in unsupported RuO_2 accounts for the role of the support on the reducibility of supported ruthenium oxide [8].

CPR20-N electrocatalyst has two reduction peaks at 50 °C and 107 °C; however, PtRu supported on non-functionalized Vulcan XC

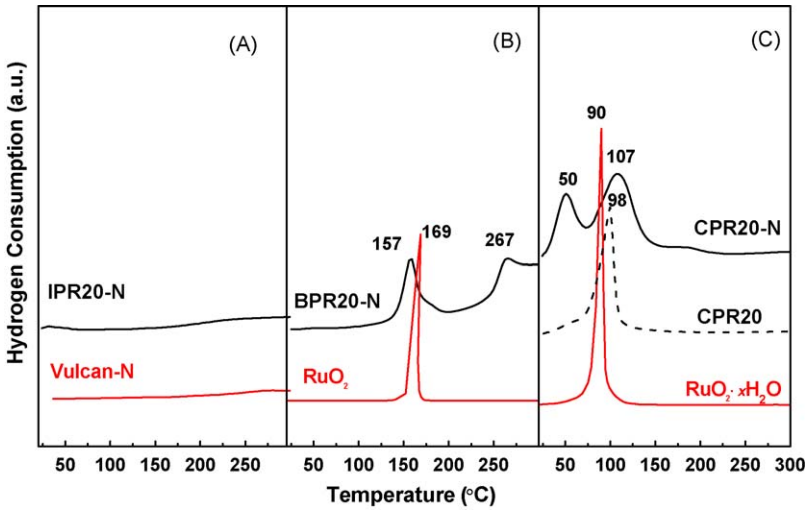

Fig. 8. TPR profiles of electrocatalysts obtained by impregnation method and Vulcan-N (A), Bonneman's method and RuO_2 (B) and sulfito-complex route and $RuO_2{\cdot}xH_2O$ (C).

72R (CPR20) displays a single hydrogen consumption process at 98 °C (Fig. 8C). TPD analysis (not shown) under H_2 confirms the lack of desorbed sulfur volatile products, which rule out the assignment of the TPR peaks to the sulfito-complex. The TPR profile of the reference $RuO_2{\cdot}xH_2O$ displays a single hydrogen consumption process at 90 °C. The two reduction peaks observed in CPR20-N suggest that a bimetallic alloy has not been obtained. According to a previous study [8], a Pt-rich surface has a lower reduction temperature than a Ru-rich surface. By comparison with the TPR of the reference, the peak at 98 °C in CPR20 could be assigned to the reduction of an amorphous $RuO_2{\cdot}xH_2O$ phase, and consequently, the TPR peaks of CPR20-N at 50 °C and 107 °C can be assigned to Pt-rich and Ru-rich surface regions, with the latter being an amorphous $RuO_2{\cdot}xH_2O$ phase. In good agreement with FTIR results, both phases should be stabilized by the oxygen-containing groups on Vulcan-N, which explains why no reduction peak attributed to the Pt-rich surface was observed in CPR20.

3.3. Electrochemical measurements

The electrooxidation of methanol on pure Pt produces adsorbed CO (CO_{ads}) that covers a considerable fraction of the electrode surface in a matter of seconds. At potentials below 0.40 V, the reaction cannot progress due to the inability of platinum to form hydroxyl groups for further CO_{ads} oxidation, and the electrical current falls to negligible values. For this reason, CO_{ad} is considered to be a catalyst "poison". Consequently, an important, albeit not unique, aspect of the catalysis of methanol oxidation is related to CO catalytic oxidation. The electrooxidation of pre-adsorbed CO (stripping technique) provides information about the material's facility for CO oxidation. In addition, the extent of this process gives information about the active surface area accessible to the reactants or electroactive area, intrinsic catalytic activity and, in some cases, catalyst surface composition. The cyclic voltammetries (CVs) during the electrooxidation of CO adsorbed on the electrocatalysts at 25 °C are given in Fig. 9. Peak potentials (E_p) for CO oxidation in BPR20-N (0.52 V) and IPR20-N (0.50 V) appear at about 0.06 V, shifted to more negative potentials than CPR20 (0.56 V) and CPR20-N (0.57 V), which record a broad peak. It would be interesting to note that the cycle recorded after CO electrooxidation on CPR20-N exhibits different absorption characteristics in the hydrogen region compared with IPR20-N, BPR-20N and CPR20 catalysts. It is known that the voltammograms of the PtRu electrodes show two competing processes in this potential region, that is, adsorption/desorption of hydrogen predominantly occurring on Pt sites and the formation of Ru–OH species [40]. Therefore, the strong hydrogen adsorption feature observed in CPR20-N catalyst suggests that different interactions between Pt and Ru surface atoms take place, which can facilitate one or both electrochemical competing processes.

In order to evaluate the methanol oxidation activity of the electrocatalysts, the cyclic voltammetry of these samples in 2 M CH_3OH/0.5 M H_2SO_4 solution, 20 mV s^{-1} and room temperature was investigated and shown in Fig. 10. The CVs of the electrocatalysts have been normalized to the electroactive area estimated from CO_{ads} stripping voltammograms. As the amount of CO_{ad} is directly related to the number of bimetallic nanoparticles, the charge involved in the process reflects the real electrochemical area of the electrode [41]. As revealed by the cyclic voltammograms depicted in Fig. 10 for electrocatalysts, methanol oxidation is extremely sensitive to the preparation method and carbon support. The catalyst obtained by the sulfito-complex route and supported on functionalized carbon is the most active. The performances of the different catalysts at potentials lower than 0.6 V decrease in the order: CPR20-N

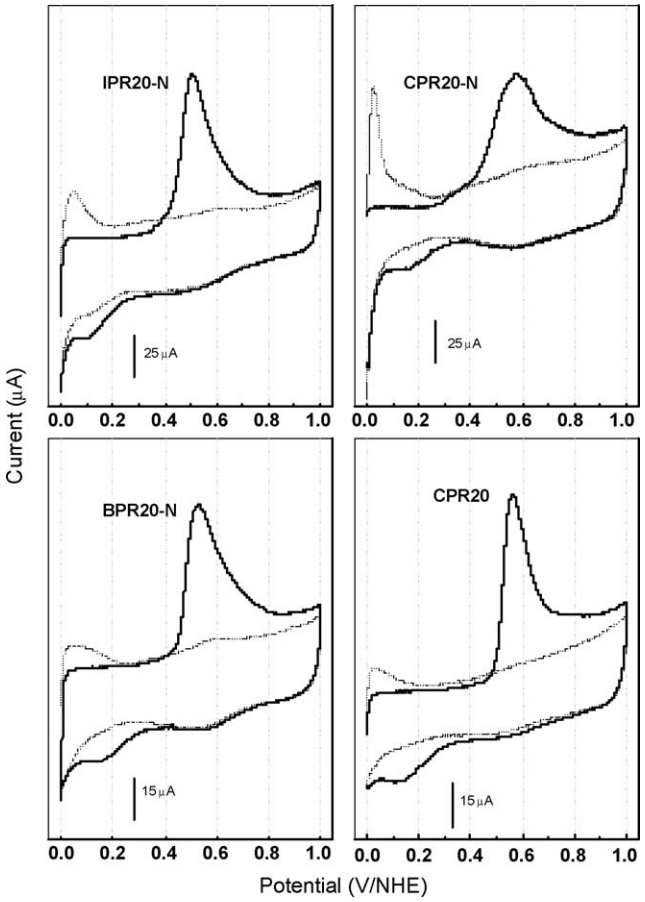

Fig. 9. CVs for the oxidation of CO in 0.5 M $HClO_4$ at 25 °C of electrocatalysts, $v = 0.02$ V s^{-1}, $E_{ads} = 0.02$ V.

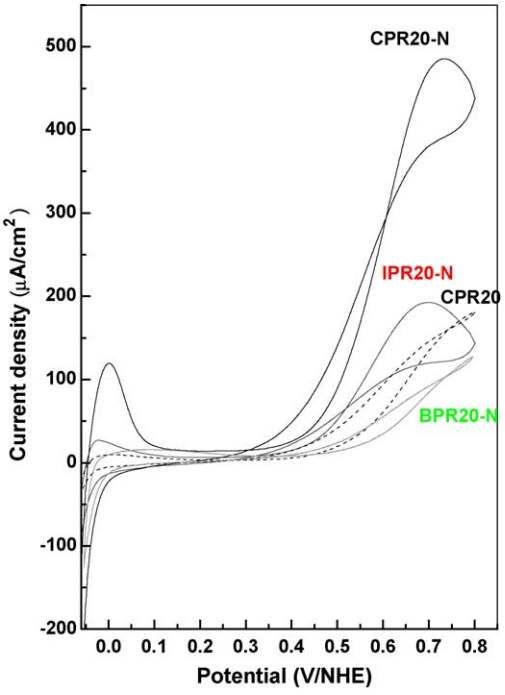

Fig. 10. CVs for the oxidation of methanol in H_2SO_4 (0.5 M) + CH_3OH (2 M) at 25 °C of electrocatalysts. Current density normalized to the electroactive area from the CO stripping analysis.

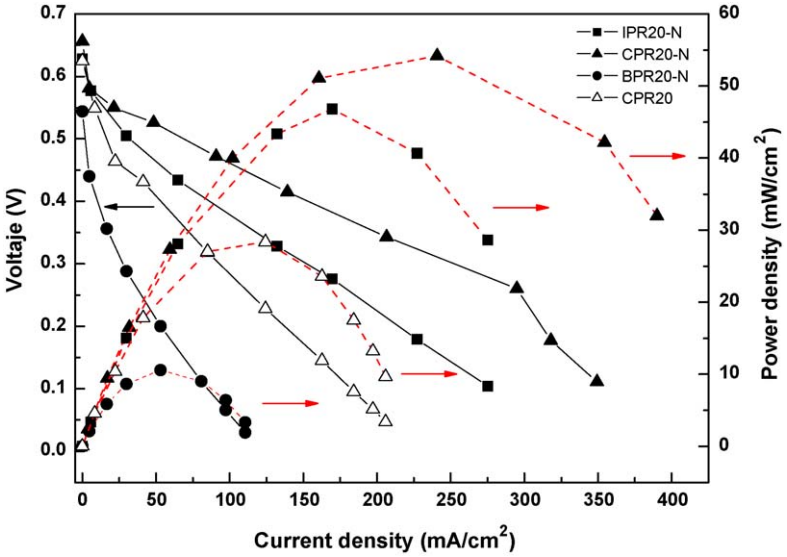

Fig. 11. DMFC performances with different anode catalysts and Pt/C (Johnson and Mattey) in the cathode operation temperature: 90 °C; methanol concentration: 2 M; flow rate: 3 mL min^{-1}; oxygen flow rate and pressure: 200 mL min^{-1}, 3 bar.

≫ IPR20-N > CPR20 > BPR20-N. For potentials lower than 0.2 V, CPR20-N catalysts again have the strong adsorption component in the hydrogen region. Nevertheless, this peak was observed only during the first scans, when the surface is free from organic residues.

3.4. DMFC performance

Electrocatalysts were tested in a single DMFC by feeding 2 M CH_3OH. Fig. 11 shows the results for electrocatalysts at 90 °C. Polarization and power density curves confirm that the efficiency of the CPR20-N catalyst is much better than IPR20-N, CPR20 and BPR20-N. Therefore, the results obtained in a half-cell at 25 °C were fully extrapolated to a single cell at 90 °C, and the higher electroactivity of CPR20-N does not seem to be affected under operating fuel cell conditions.

These results show that the preparation method and nature of the carbon support are crucial factors in determining the electroactivity of electrocatalysts. Structural characteristics such as chemical state, degree of alloying, type of crystal phases, metal–support interaction seem to play an important role in methanol electrooxidation. The low activity of BPR20-N is due to the presence of metal precursor traces and the formation of crystalline RuO_2 that are not electrochemically active [42]. Moreover, tetragonal RuO_2 remains electrochemically unchanged during methanol oxidation, and could block active sites on the electrocatalyst surface. The changes in hydrophobicity of the carbon upon treatment with HNO_3 are important because acid groups are introduced into the carbon. These surface groups increase the wettability of the carbon, facilitating the access of the metal precursor in aqueous solution, but hinder the access of anhydrous metal precursors in non-polar solvents during synthesis. The metal precursor distribution throughout the functionalized carbon support is an important aspect, where solvent–carbon interactions play a major role. Once the metal precursor has been distributed on the carbon support, the maintenance of this distribution during the reduction stage is important. Surface oxygen-containing groups of the support seem to be unable to stabilize the anhydrous precursors of platinum and ruthenium in a catalyst obtained by Bönnemann's method, which could be the reason that precursors and crystalline RuO_2 were observed in BPR20-N catalyst.

The high activity of CPR20-N could be attributed to the formation of hydrous ruthenium oxide, stabilized by functionalized support, according to TPR profiles. The nanoparticles appear uniformly distributed over the carbon surface, probably attached to specific surface sites or etch pits created by the carbon oxidation treatment, consistent with FTIR measurements. The presence of hydrous ruthenium oxide in CPR20-N catalysts has been verified by XPS and TPR analysis, but not by XRD, suggesting that these species are present in the catalysts as amorphous materials, not detectable by X-ray diffraction.

An important topic of contemporary discussion is whether a PtRu alloy is needed to obtain the desired improvement in methanol electrooxidation or if the mere presence of Ru next to electrocatalytically active Pt centers is sufficient to improve fuel cell performance. It is noteworthy that in our tailored PtRu samples, preparation method plays an important role in deciding the local structure around Pt atoms, where alloy formation does not seem to be an essential requirement for a superior electrocatalytic performance as long as close contact is achieved between platinum and $RuO_2{\cdot}xH_2O$ phases. This result is consistent with Rolison's observation that the bimetallic alloy is not the most desired form of catalyst, and $RuO_2{\cdot}xH_2O$ is a much more active catalyst for methanol oxidation than Ru^0 [18,19]. However, the activity of CPR20 as methanol oxidation electrocatalyst is lower than that of CPRN-20 recorded under similar reaction conditions. This feature suggests that the presence of $RuO_2{\cdot}xH_2O$ phase alone is not enough to justify the performance of the electrocatalysts, and factor others than this should be taken into consideration.

Size effects are actively discussed, where optimal size for methanol electrooxidation is typically considered to be 2–3 nm [15]. Takasu et al. [7] reported the low activity of small (≤2 nm) PtRu particles, which was attributed to the "negative" particle size effect, due to their low intrinsic catalytic activity and susceptibility to poisoning [43]. Additionally, gradual changes in particle size over the course of catalyst operation have been mentioned in many papers even for relatively short experimental tests. In our catalysts, IPR20-N shows an average particle size of 3.7 nm, with a broader size distribution than catalysts obtained by colloidal methods. However, the electrocatalytic activity towards methanol oxidation of IPR20-N is higher than BPR20-N and CPR20 (average particle size ca. 2 nm) and lower than CPR20-N (Fig. 4). Therefore, the existence

and sign of size effect is not found in catalysts with similar metal loading and Pt/Ru atomic ratio, and other morphological variations attributed to the modification of the surface chemistry of the carbon and precursor–support interaction may play a more important role.

At present, the methanol oxidation mechanism is still not fully understood, a factor which is hindering the development of DMFC. When discussing the reason for the enhanced rate of methanol oxidation on PtRu, the bifunctional mechanism is often invoked [6]. The term was suggested to emphasize the joint activities of both metals, with Pt being the one adsorbing and dissociating methanol and Ru the one oxidizing the adsorbed residues at low potentials [44]. The mechanism is described forthwith in a simplified manner. The adsorbed OH^- is formed at ruthenium sites in a lower potential range according to:

$$Ru + H_2O \rightarrow Ru{-}(OH)_{ads} + H^+ + e^-$$

The bifunctional approach assumes that Ru promotes the oxidation of the strongly bonded CO on Pt by supplying an oxygen source, following a Langmuir–Hinschelwood mechanism:

$$Pt{-}(CO)_{ads} + Ru{-}(OH)_{ads} \rightarrow Pt + Ru + CO_2 + H^+ + e^-$$

It is clear that modification of the adsorbed OH^- coverage in Ru atoms is essential for the improvement of the overall oxidation rate. Rolison and co-workers [18,19] emphasized the importance of hydrous ruthenium oxides because the $RuO_2{\cdot}xH_2O$ speciation of Ru in nanoscale PtRu blacks records both high electron and proton conductivity. In addition, $RuO_2{\cdot}xH_2O$ has important mechanistic implications for direct methanol oxidation, because $RuO_2{\cdot}xH_2O$ is mixed +3/+4 valent and innately expresses Ru–OH speciation, as denoted by the following equation [45]:

$$Ru^{4+}{-}O^{2-} + H^+ + e^- \leftrightarrow Ru^{3+}{-}OH^-$$

The presence of Ru(+4) species in highly dispersed PtRu/C samples was estimated for Hamnett and co-workers [42] in a ^{99}Ru Mössbauer study. They found that Ru is present as a mixture of inactive anhydrous tetragonal RuO_2 and other active form of Ru(+4), which facilities oxygen spillover from ruthenium to platinum. This active form of Ru(+4) can be associated with the $RuO_2{\cdot}xH_2O$ phase, whose electrochemical and electrocatalytic properties depend on the amount of water in its structure [27]. These unusual electrochemical properties of $RuO_2{\cdot}xH_2O$ should be related to the atomic structure of the material. As deduced by the lack of reflection in powder XRD in the characterization of the catalysts of the present work, hydrous RuO_2 is amorphous. Hydrous RuO_2 has been reported to chemisorb a significant amount of oxygen, whereas the anhydrous form adsorbs little oxygen. These differences might greatly affect the activity of RuO_2 in the oxidation of alcohols. Consequently, the oxygen surface groups of the carbon support may play an important role in the properties of hydrous RuO_2. The increase in the number of oxygen surface groups may favor the presence of a sufficient concentration of adsorbed oxygenated species at its surface at low potential, and in addition could facilitate the easy removal of poisoning species. Moreover, the intense surface oxidation of the carbon may produce an increase in the interaction between the $RuO_2{\cdot}xH_2O$ and the support, thus increasing the stability of these species during the electrochemical process.

These results indicate that a deeper knowledge of the chemical nature of the carbon support is needed in carbon-supported PtRu electrocatalysts, since its effect on the final properties may be at least as important as other more studied factors, such as the preparation method.

4. Conclusions

PtRu nanoparticles supported on carbon functionalized with HNO_3 were prepared via impregnation, Bönnemann's method and the sulfito-complex route. X-ray diffraction and TPR measurements evidence the presence of $RuO_2{\cdot}xH_2O$ phases in the catalyst obtained by the sulfito-complex route. This species is stabilized by metal–support interaction. Alloy characteristics were estimated for PtRu catalyst obtained by impregnation and Bönnemann's method. Surface oxygen-containing groups of the support seem to be unable to stabilize the anhydrous precursors of platinum and ruthenium in catalysts obtained by Bönnemann's method, which yield crystalline RuO_2. Although all catalysts show similar CO tolerance, a rather different methanol electrooxidation performance is observed. The combination of the electrocatalytic nature of $RuO_2{\cdot}xH_2O$ species and functionalized carbon black in catalysts obtained by the sulfito-complex route greatly improves the performance in a single DMFC. These results demonstrate that the synthetic route and the nature of the carbon support are crucial factors in determining the electroactivity of electrocatalysts.

Acknowledgement

This research was funded by the Ministry of Education and Science, Spain (Project ENE2007-67533-C02-01).

References

[1] S. Wasmus, A. Küver, J. Electroanal. Chem. 461 (1999) 14–31.
[2] A.S. Aricò, R. Srinivasan, V. Antonucci, Fuel Cells 1 (2001) 133–161.
[3] R. Dillon, S. Srinivasan, A.S. Arico, V. Antonucci, J. Power Sources 127 (2004) 112–126.
[4] H. Liu, C. Song, L. Zhang, J. Zhang, H. Wang, D.P. Wilkinson, J. Power Sources 155 (2006) 95–110.
[5] O. Petrii, J. Solid State Electrochem. 12 (2008) 609–642.
[6] M. Watanabe, S. Motoo, J. Electroanal. Chem. 60 (1975) 267–272.
[7] Y. Takasu, H. Itaya, T. Iwazaki, R. Miyoshi, T. Ohnuma, W. Sugimoto, Y. Murakami, Chem. Commun. (2001) 341–342.
[8] S.Y. Huang, S.M. Chang, C. Yeh, J. Phys. Chem. B 110 (2006) 234–239.
[9] B. Yang, Q.Y. Lu, Y. Wang, L. Zhuang, J.T. Lu, P.F. Liu, Chem. Mater. 15 (2003) 3552–3557.
[10] J.L. Gómez de la Fuente, M.V. Martínez-Huerta, S. Rojas, P. Terreros, J.L.G. Fierro, M.A. Peña, Catal. Today 116 (2006) 422–432.
[11] L.H. Jiang, G.Q. Sun, X.S. Zhao, Z.H. Zhou, S.Y. Yan, S.H. Tang, G.X. Wang, B. Zhou, Q. Xin, Electrochim. Acta 50 (2005) 2371–2376.
[12] W.H. Lizcano-Valbuena, D.C. de Azevedo, E.R. Gonzalez, Electrochim. Acta 49 (2004) 1289–1295.
[13] M. Watanabe, M. Uchida, S. Motoo, J. Electroanal. Chem. 229 (1987) 395–406.
[14] H. Bönnemann, W. Brijoux, R. Brinkmann, R. Fretzen, T. Joussen, R. Köppler, B. Korall, P. Neiteler, J. Richter, J. Mol. Catal. 86 (1994) 129–177.
[15] A. Hamnett, Catal. Today 38 (1997) 445–457.
[16] D. Chu, S. Gilman, J. Electrochem. Soc. 143 (1996) 1685–1690.
[17] G. Wu, L. Li, B.Q. Xu, Electrochim. Acta 50 (2004) 1–10.
[18] J.W. Long, R.M. Stroud, K.E. Swider-Lyons, R. Rolison, J. Phys. Chem. B 104 (2000) 9772–9776.
[19] D.R. Rolison, P.L. Hagans, K.E. Swider, J.W. Long, Langmuir 15 (1999) 774–779.
[20] Z.G. Chen, X.P. Qiu, B. Lu, S.C. Zhang, W.T. Zhu, L.Q. Chen, Electrochem. Commun. 7 (2005) 593–596.
[21] L. Cao, F. Scheiba, C. Roth, F. Schweiger, C. Cremers, U. Stimming, H. Fuess, L.Q. Chen, W.T. Zhu, X.P. Qiu, Angew. Chem. Int. Ed. 45 (2006) 5315–5319.
[22] M.K. Jeon, J.Y. Won, S.I. Woo, Electrochem. Solid State Lett. 10 (2007) B23–B25.
[23] Y. Otake, R.G. Jenkins, Carbon 31 (1993) 109–121.
[24] V.M. Jovanovic, S. Terzic, A.V. Tripkovic, K.Dj. Popovic, J.D. Lovic, Electrochem. Commun. 6 (2004) 1254–1258.
[25] Z.B. Wang, G.P. Yin, P.F. Shi, Carbon 44 (2006) 133–140.
[26] J.L. Gómez de la Fuente, M.V. Martínez-Huerta, S. Rojas, P. Terreros, J.L.G. Fierro, M.A. Peña, Carbon 43 (2005) 3002–3005.
[27] T.L. Stuchinskaya, M. Musawir, E.F. Kozhevnikova, I.V. Kozhevnikov, J. Catal. 231 (2005) 41–47.
[28] T.J. Schmidt, M. Noeske, H.A. Gasteiger, R.J. Behm, P. Britz, H. Bönnemann, J. Electrochem. Soc. 145 (1998) 925–931.
[29] Z. Qi, A. Kaufman, J. Power Sources 113 (2003) 37–44.
[30] J. Prabhuram, T.S. Zhao, H. Yang, J. Electroanal. Chem. 578 (2005) 105–116.
[31] J.S. Noh, J.A. Schwarz, Carbon 28 (1990) 675–682.
[32] C. Prado-Burguete, A. Linares-Solano, F. Rodríguez-Reinoso, C. Salinas-Martínez de Lecea, J. Catal. 115 (1989) 98–106.

[33] J.L. Figueiredo, M.F.R. Pereira, M.M.A. Freitas, J.J.M. Órfao, Carbon 37 (1999) 1379–1389.
[34] K.H. Kangasniemi, D.A. Condit, T.D. Jarvi, J. Electrochem. Soc. 151 (2004) E125–E132.
[35] D. Briggs, M.P. Seah, Practical Surface Analysis by Auger and X-ray Photoelectron Spectroscopy, Wiley, 1990.
[36] A.S. Arico, V. Baglio, A. Di Blasi, E. Modica, P.L. Antonucci, V. Antonucci, J. Electroanal. Chem. 557 (2003) 167–176.
[37] E. Cano-Serrano, J.M. Campos-Martin, J.L.G. Fierro, Chem. Commun. (2003) 246–247.
[38] K.W. Wang, S.Y. Huang, C.T. Yeh, J. Phys. Chem. C 111 (2007) 5096–5100.
[39] C.G. Michel, W.E. Bambrick, R.H. Ebel, Fuel Process. Technol. 35 (1993) 159–182.
[40] E. Ticanelli, J.G. Beery, M.T. Paffett, S. Gottesfeld, J. Electroanal. Chem. 258 (1989) 61–77.
[41] H.A. Gasteiger, N.M. Markovic, P.N. Ross Jr., E.J. Cairns, J. Phys. Chem. 98 (1994) 617–624.
[42] A. Hamnett, B.J. Kennedy, F.E. Wagner, J. Catal. (1990) 30–40.
[43] A.N. Gavrilov, E.R. Savinova, P.A. Simonov, V.I. Zaikovskii, S.V. Cherepanova, G.A. Tsirlina, V.N. Parmon, Phys. Chem. Chem. Phys. 9 (2007) 5476–5489.
[44] T. Iwasita, in: W. Vielstich, H.A. Gasteiger, A. Lamm (Eds.), Handbook of Fuel Cells. Fundamental Technology and Applications., vol. 2, Wiley, Chichester, 2003, pp. 603–624.
[45] W. Dmowski, T. Egami, K.E. Swider-Lyons, C.T. Love, D.R. Rolison, J. Phys. Chem. B 106 (2002) 12677–12683.